Full Paper

Wiley Online Library

ELECTROANALYSIS

DOI: 10.1002/elan.201800115

# Electroanalysis of an Iron@Graphene-Carbon Nanotube Hybrid Material

Dayana Soto,[a] Manuela Alzate,[b] Jaime Gallego,[b] and Jahir Orozco*[a]

**Abstract:** Hybrid nanomaterials have outstanding properties that are superior to the corresponding constituents working alone. This work reports on the electroanalysis of a hybrid material-decorated screen-printed carbon electrode (SPCE) that consists of iron nanoparticles supported at multi-wall carbon nanotubes (MWCNT), coated with graphene layers, named Fe@G-MWCNT. Electrochemical and morphological characterizations were carried out by cyclic voltammetry, electrochemical impedance spectroscopy and high-resolution transmission electron microscopy, respectively. After optimizing the amount of hybrid material to be drop casted at the SPCE, its electrochemical activation in sulphuric acid produced an enhanced response. The resultant electrochemically reduced Fe@G-MWCNT-e-modified electrode exhibited a diffusion-controlled redox process with an enhanced heterogeneous electron-transfer rate constant of $3.21 \times 10^{-2}$ cm·s$^{-1}$, which was superior to that from the MWCNT counterpart. However, it was slightly lower than that from a Fe-MWCNT-decorated electrode. The graphene coating limited slightly the electron-transfer process, but works as a protective layer that prevent the loss of Fe catalytic activity. The electrochemical response of the hybrid with graphene coated Fe decreased only a 24.3% after one week, respect to 51.9% of the uncoated one. In addition, the hybrid material-modified electrode exhibited electrocatalytic activity towards the reduction of $H_2O_2$ in a linear range of 0.5 mM to 9.8 mM, with sensitivity of 7.97 μA·mM$^{-1}$ and LOD of 0.65 mM, thereby opening an avenue for the development of more specific and highly sensitive Fe@G-MWCNT hybrid-based (bio) sensors.

**Keywords:** Electroanalysis · Hybrid material · Multi-wall carbon nanotube · Graphene · Screen-printed carbon electrode

## 1 Introduction

Nanostructured hybrid materials have been increasingly exploited in the development of a variety of devices, including supercapacitors, dye sensitized solar cells, batteries and (bio) sensors [1]. In particular, such nano-bioengineered architectures may enable the development of transducer platforms of improved electrochemical performance [2], and functional interfaces. For the construction of electroactive sensing platforms of enhanced properties, a myriad of organic-inorganic hybrid materials have been proposed [3–7]. Hybrid materials combine organic and inorganic building blocks, which working together generate a synergic effect of improved performance with respect to the individual components acting alone [8].

Carbon nanomaterials (CNM) have gained attention as a supporting material in functional interfaces because of their high surface area, electrical conductivity and adsorption, as well as their high mechanical, thermal and chemical stability; and relative biocompatibility [7,9–12]. In the development of biosensors, other nanomaterials and bioreceptors are incorporated along with CNM [9,13–16] to lower overvoltage and accelerate electrode kinetics; and to obtain selectivity, respectively [17,18].

Among CNM, carbon nanotubes (CNT) and graphene are nanomaterials widely explored in the development of nanobioengineered platforms because of their unique structural and physicochemical properties [19–22]. For example, multi-walled carbon nanotubes (MWCNT) have been broadly interrogated for chemical and biological sensing applications [23–26]. They are hollow cylinders of multiple layers of graphite superimposed and rolled. The graphite layers are composed of conjugated sp$^2$-hybridized carbon atoms arranged into a planner 2D honeycomb lattice [27]. However, the electrical conductivity of MWCNTs is affected by the non-uniform contact and discontinuities or defects of nanomaterials, thereby limiting their applications in (bio) sensors [23].

Metallic nanoparticles have been used in electrochemical biosensor devices to improve their conductive properties. They can mediate fast electron-transfer processes and promote a better contact between bioreceptors and transducers, thus improving the sensitivity of the resultant devices [28,29]. Iron nanoparticles are partic-

[a] D. Soto, J. Orozco
Max Planck Tandem Group in Nanobioengieneering, Universidad de Antioquia, Complejo Ruta N, Calle 67 N° 52–20, Medellín 050010, Colombia
E-mail: grupotandem.nanobioe@udea.edu.co
[b] M. Alzate, J. Gallego
Química de Recursos Energéticos y Medio Ambiente, Instituto de Química, Universidad de Antioquia, Calle 70 N° 52–21, Medellin, Colombia

Supporting information for this article is available on the WWW under https://doi.org/10.1002/elan.201800115

ularly attractive because of their biocompatibility, higher bioactivity and conformation stability [30,31]. However, the implementation of inorganic particles in (bio) sensors is limited by changes in their oxidation state because of variations in conditions of the medium such as pH and temperature. Herein, we hypothesize that coating metal particles with graphene sheets can be an attractive option for the generation of chemically stable materials with steady conductive properties and catalytic activity.

Graphene is a two-dimensional structure that comprises a single layer of $sp^2$-hybridized carbon atoms joined by covalent bonds to form a hexagonal lattice. Graphene's structure is never atomically flat as a result of its high flexibility, and the tendency of graphene sheets to curling, folding and corrugating [22]. Coating metals with graphene sheets generates core-shell-like type structures with high chemical stability and low cytotoxicity, but with some hindering of their catalytic activity [23].

In this work, we studied the electrochemical performance of a SPCE modified with a hybrid material based on MWCNT decorated with iron nanoparticles, which were in turn encapsulated into few layers of graphene (Fe@G-MWCNT). This is the first time that this new hybrid material is electrochemically characterized. Exhaustive characterization by cyclic voltammetry (CV) and Electrochemical Impedance Spectroscopy (EIS) showed the Fe-decorated MWCNT has superior electrochemical properties than the Fe@G-MWCNT and the MWCNT counterparts alone. Furthermore, we demonstrated that the thin graphene flakes can work as a protective layer, preventing the loss of the catalytic properties of the Fe nanoparticles, and thus improving the long-term stability of the hybrid material. Overall, the hybrid material holds potential for the construction of electrochemical biosensors of improved sensitivity, high biocompatibility, and long-term stability.

## 2 Experimental

### 2.1 Reagents and Solutions

Potassium ferricyanide (III) ($K_3[Fe(CN)_6]$), potassium hexacyanoferrate (II) trihydrate ($K_4[Fe(CN)_6]\cdot 3H_2O$) and hydrogen peroxide ($H_2O_2$) 30% were purchased from Merck Millipore. Potassium nitrate ($KNO_3$), dipotassium hydrogen phosphate ($K_2HPO_4$) and disodium hydrogen phosphate ($Na_2HPO_4$) were acquired from Panreac AppliChem. Potassium dihydrogen phosphate ($KH_2PO_4$), potassium chloride (KCl) and sodium chloride (NaCl), were purchased from J. T Baeker. Sulphuric acid ($H_2SO_4$) was acquired from Fluka™. All reagents were used as received and the solutions were prepared using de-ionized water of 18 mΩ·cm from a Smart2Pure 3 UV/UF Milli-Q system.

### 2.2 Materials and Instruments

Morphology and size of metallic nanoparticles and the Fe@G-MWCNT hybrid material were determined by high resolution transmission electron microscopy (HR-TEM) using a JEOL 2110 UHR instrument, at 200 kV accelerating voltage. The powder material was suspended in ethanol by sonication and deposited on a TEM lacey carbon grid.

SPEs purchased from DropSens (ref. 110, DS SPCE) were employed as supporting electrodes. They include a three-electrode cell configuration printed on the same strip. The strips consist of a 4 mm working electrode, a counter electrode (both of them printed using heat curing carbon composite inks), and a silver pseudo-reference electrode, respectively.

All the electrochemical measurements were performed in a potentiostat/galvanostat and impedance analyser PalmSens3 with software PSTrace4 version 4.8.1.

### 2.3. Preparation the Fe@G-MWCNT Hybrid Material

The hybrid was rationally designed and fabricated by accommodating the different materials, in a sequential and controlled manner as follow. MWCNT were obtained through an ethanol decomposition reaction process at 900 °C in presence of perovskites ($LaFeO_3$) as catalyst precursors [21]. The catalyst was placed into a horizontal reactor; temperature was raised at 10 °C·min$^{-1}$ under $N_2$ atmosphere until the desired reaction temperature, for 4 h. The MWCNT obtained were treated with 65% $HNO_3$ and 96% $H_2SO_4$ (3:1), for 15 min at 130 °C, by applying a power of 500 W in a Milestone MicroSYNTH microwave. The product was filtered and washed with deionized water until neutral pH. The residue was then dried at 100 °C for 24 h [32].

The treated MWCNTs were decorated with iron nanoparticles (Fe-MWCNT) through the metal impregnation method as previously reported [21]. Briefly, carbon nanotubes were dispersed into an iron nitrate solution to obtain a nominal mass fraction of 10% of Fe, over MWCNT, using an ultrasound bath. The pH of the dispersion was adjusted by addition of a pH 9.5, 2.5% $NH_3$ solution under constant magnetic stirring, for 30 min. The material was washed and dried for 24 h in a conventional oven at 100 °C.

The Fe-MWCNT material was coated with some graphene layers. For this purpose, the Fe-MWCNTs were placed into a vertical quartz reactor under argon atmosphere at 100 mL·min$^{-1}$ until 900 °C, in order to decompose the nitrates and reduce the metal. When the reaction temperature was reached, 100 mL pulses of pure methane were injected into the reactor. The Fe@G-MWCNT hybrid material was then obtained.

### 2.4 Fabrication of the Hybrid Material-Decorated SPCE

Initially, an electrochemical pre-treatment of the SPCEs was carried out by chronoamperometry in a pH 7.4, 0.05 M phosphate buffer, at a fix potential of +1.6 V, for 4 min [33]. The electrochemical performance of the activated SPCE were verified through CV in a 1 mM $K_4[Fe(CN)_6]$/0.1 M $KNO_3$ solution; in the range of 0.4 V to −0.2 V at 0.05 V·s$^{-1}$ scan rate, for two consecutive cycles. The shape of the voltammetric curve in this solution along with the current recorded are useful to confirm the effective removal of residual materials and the suitable electrochemical performance of the pre-treated SPCEs.

Later, 4.0 μL of an aqueous dispersion of hybrid materials were drop casted onto the surface of the working electrode of the pre-treated SPCEs and incubated overnight in a wet chamber. After the hybrid material adsorption, the electrodes were rinsed with Milli-Q water (3 times) and allowed to dry at ambient temperature.

Finally, the hybrid materials were electrochemically activated in 0.1 M $H_2SO_4$ by successive CV, scanning between 0.5 V and 1.0 V (at 50 mV·s$^{-1}$), for 10 cycles, to obtain the electrochemically active materials, named Fe-MWCNT-e and Fe@G-MWCNT-e [34].

Evaluation of the electrochemical performance of the modified SPCE was achieved by CV in $H_2O_2$, with a scanning rate of 50 mV·s$^{-1}$, from 0.5 V to −1.0 V. EIS was conducted at 0.16 V and 0.005 V of amplitude, with a frequency range of 50 kHz–0.01 Hz. The impedance data was fitted using ZView software (version 3.5d). Chronoamperometry measurements were recorded at a potential of −0.68 V for 4 min, after a pre-conditioning step of 10 s, at an open circuit potential.

## 3 Results and Discussion

### 3.1 Morphology of the Hybrid Material

The hybrid material based on MWCNT decorated with Fe and coated with graphene was synthetized according with an already reported procedure [21], and the morphology was studied herein by using TEM. Figure 1 shows TEM micrographs of the resultant hybrid material. The MWCNTs appear as a tubular-like, randomly cross-linked structure, supporting some well-defined, round nanoparticles. The inset from Figure 1a shows Fe metallic nanoparticles with an average particle size of 18 nm ± 9 nm (n = 50). Figure 1b is a closed-up image of a MWCNT-supported metallic Fe nanoparticle coated with some graphene thin flakes coating its surface. From this micrograph, it is possible to distinguish the different crystal planes corresponding to the MWCNT, Fe and graphene materials, demonstrating that the three of them are coexisting as a hybrid material. Unlike MWCNT-embedded Fe nanoparticles commonly reported, in our hybrid material, the Fe nanoparticles are decorating the MWCNT surface, being more exposed, thereby favoring the Fe catalytic activity and the faster electrochemical response of the hybrid material. The metallic nanoparticles were well-wrapped within the graphene thin sheets, from the intrinsic impregnation-reduction-decoration fabrication process [21]. The graphene coating surface seems to be rougher than the bare MWCNT, which is related with the curling and corrugated graphene sheets.

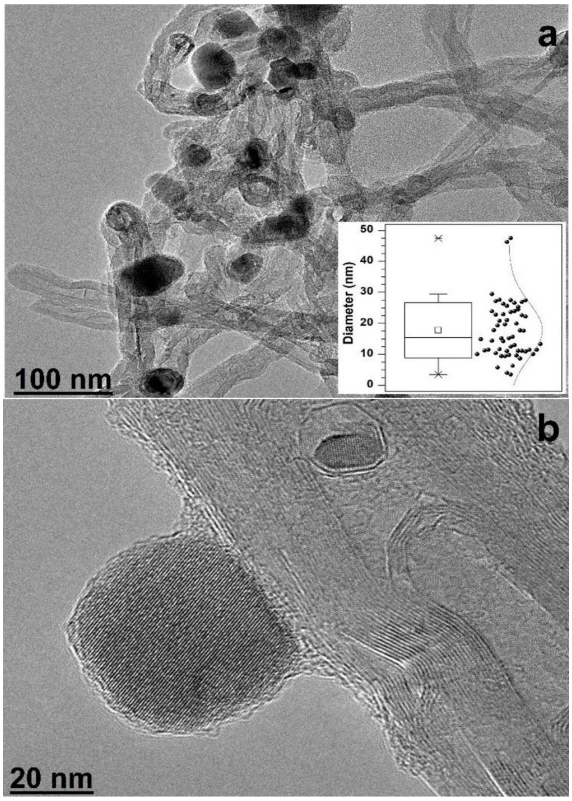


Fig. 1. TEM micrographs of **(a)** Fe-MWCNT network and **(b)** Fe@G-MWCNT. Inset is the iron metal particle size histogram, with n = 50.

### 3.2 Electrochemical Study of MWCNT Concentration as a Supporting Material

SPCEs are cheap, require small sample volume and their sensitivity/selectivity can be enhanced easily by deposition of suitable (bio) materials on their surface. Herein, to modify the electrodes, different concentrations of MWCNT ranging from 0.1 mg·mL$^{-1}$ to 1.0 mg·mL$^{-1}$ were drop casted at the surface of the SPCE.

The electrochemical response was evaluated by both CV and EIS, following the protocol described in the Experimental Section 2.4. Figure 2a shows how current intensity of the oxidation and reduction peaks from the electrochemical probe increases with increasing concentrations of hybrid material in the range of 0.1 mg·mL$^{-1}$ to 0.5 mg·mL$^{-1}$ (Table 1). Such an increase indicates both, the proper deposition of MWCNTs at the electrode surface and that the presence of the MWCNT promotes

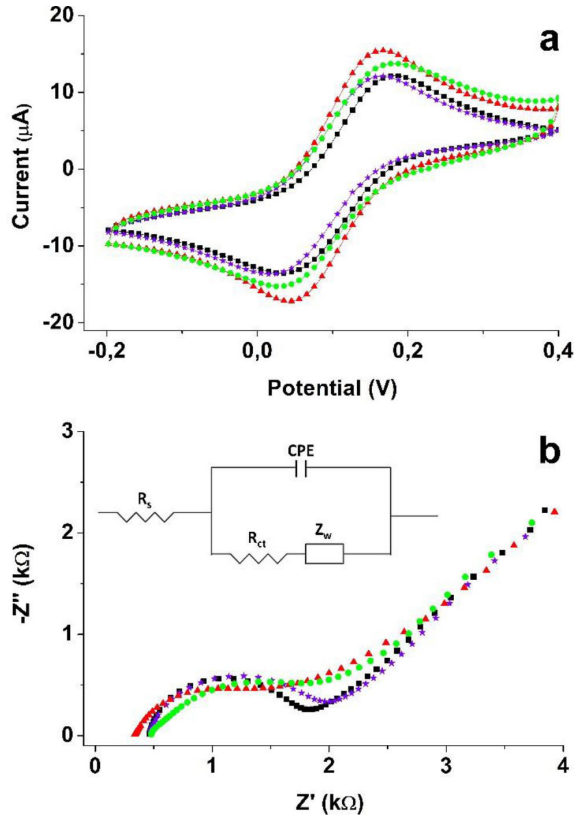


Fig. 2. **(a)** Cyclic voltammograms of MWCNT-modified SPCE in a 1 mM $[Fe(CN)_6]^{3-}$/0.1 M $KNO_3$ solution. **(b)** Nyquist plot in a pH 7.4, 5 mM $[Fe(CN)_6]^{4-/3-}$/PBS 1X solution, in the frequency range from 50 kHz to 0.01 Hz, at an amplitude of 0.005 V. SPCE modified with increasing concentrations of MWCNT, 0.0 (■), 0.1 (★) mg·mL$^{-1}$, 0.5 (▲) mg·mL$^{-1}$ and 1.0 (●) mg·mL$^{-1}$. Inset is the equivalent circuit that represents the parameters from the electrochemical system.

the charge-transfer process respect to the bare SPCE, as expected. However, for a concentration of 1.0 mg·mL$^{-1}$ the current response decreases, which may be related to the formation of material multilayers that limit the electron-transfer, as will be demonstrated by EIS measurements.

EIS is a very sensitive analytical tool used to study the interfacial properties of surface-modified electrodes, among other uses. Electrochemical impedance properties of the MWCNT-modified SPCEs were tested in a pH 7.4, 5.0 mM $[Fe(CN)_6]^{4-/3-}$/PBS 1X solution, which are represented as a Nyquist plot ($-Z''$ vs. $Z'$) in Figure 2b. The inset of Figure 2b shows the Randles equivalent circuit model used to fit the experimental data. $R_{ct}$ is the charge transfer resistance, $R_s$ is the electrolyte resistance, $Z_w$ is the Warburg diffusion element and *CPE* is the constant phase element, replacing herein the typical double layer capacitance to take into account the topological imperfections of the electrode surface and fit better the experimental data [23,35,36].

In the Randles equivalent circuit model $R_{ct}$ and *CPE* are placed in parallel and represent the electrode impedance [34]. The semicircle part from the Nyquist plot corresponds to $R_{ct}$ and $R_s$ at lower frequencies; and the linear part, at higher frequencies, corresponds to the diffusion process [37,38] at the modified and bare SPCE, respectively. The lower semicircle from MWCNT-0.5-modified SPCE respect to that from other concentrations of modified materials and to the bare SPCE indicate the lower resistance that the material is offering to the current pass. These results agree to those from the CV, where MWCNT-0.5-modified SPCE led to the higher current intensity of the oxidation and reduction peaks and less peak separation, as discussed above. The very small values of Chi-squared function ($\chi^2$) for the best-fit Randle's equivalent circuit, lower than $1.3\times10^{-3}$, demonstrated that the fitted curve agreed to the experimental data. All EIS parameters are given in Table 1. The resistance caused by charge-transfer dropped from ~1426 Ω down to ~1205 Ω for the bare electrode and the MWCNT-0.5-modified surface, respectively. This is associated with changes in the electrical properties of the electrode surface as a result of decoration with CNTs (Table 1). All other modifications of SPCE led to higher $R_{ct}$, and thus MWCNT-0.5

Table 1. Electrochemical characterization of the modified electrodes. Data from Cyclic voltammetry experiments (left side): Peak anodic current intensity (**$I_{p,a}$**), anodic and cathodic peak separation (**ΔEp)**, electroactive area (**A**) and heterogeneous electron-transfer rate constant (**$k_s$**). Data from EIS experiments (right side): Charge-transfer resistance (**$R_{ct}$**), electrolytic solution resistance (**$R_s$**), Warburg diffusion element (**$Z_w$**), constant phase element (**CPE**) with pre-exponential factor (**P**) and exponent (**n**) and Chi-squared function ($\chi^2$).

| Data from cyclic voltammetry experiments | | | | | Equivalent circuit elements from the EIS experiments | | | | | |
|---|---|---|---|---|---|---|---|---|---|---|
| Electrode Type | Ip,a (μA) | ΔEp (mV) | A (mm$^2$) | ks (cm·s$^{-1}\times10^{-2}$) | Rct (Ω) | Rs (Ω) | Zw (Ω) | CPE P (F) | n | χ2 |
| SPCE | 11.5 ± 0.6 | 123.7 ± 2.9 | 7.1 ± 0.3 | 1.20 | 1426.0 | 455.1 | 1363.0 | $7.4\times10^{-6}$ | 0.85 | $1.6\times10^{-3}$ |
| MWCNT-0.1 | 11.9 ± 0.2 | 122.0 ± 8.7 | 7.4 ± 0.1 | 1.24 | 1324.0 | 469.3 | 1331.0 | $8.4\times10^{-6}$ | 0.87 | $1.8\times10^{-4}$ |
| MWCNT-0.5 | 13.9 ± 0.1 | 103.7 ± 2.9 | 8.6 ± 0.1 | 1.27 | 1205.0 | 335.2 | 1028.0 | $3.6\times10^{-5}$ | 0.76 | $2.0\times10^{-4}$ |
| MWCNT-1.0 | 11.4 ± 0.3 | 118.7 ± 10.4 | 7.1 ± 0.2 | 1.27 | 1218.0 | 463.5 | 845.6 | $1.1\times10^{-4}$ | 0.62 | $5.2\times10^{-3}$ |
| Fe-MWCNT-e | 17.2 ± 0.1 | 89.7 ± 3.2 | 10.6 ± 0.1 | 5.29 | 1041.0 | 434.4 | 521.2 | $2.3\times10^{-4}$ | 0.52 | $6.5\times10^{-4}$ |
| Fe@G-MWCNT-e | 16.7 ± 0.3 | 86.7 ± 5.5 | 10.3 ± 0.2 | 3.21 | 1181.0 | 388.1 | 737.3 | $1.3\times10^{-4}$ | 0.61 | $1.6\times10^{-3}$ |

(0.5 mg·mL$^{-1}$) was selected as optimal concentration for the subsequent experiments.

### 3.3 Electrochemical Characterization of the Hybrid Material

To characterize the hybrid material-modified surface, we studied the electrochemical changes occurring at each stage of the electrode decoration. For example, the electrochemical response of the bare SPCE, and that after deposition of MWCNT, Fe-MWCNT, Fe-MWCNT-e and Fe@G-MWCNT-e were studied by CV (Figure 3a). The quasi-reversible one electron redox transference of $[Fe(CN)_6]^{4-/3-}$ ions was observed at the optimal MWCNT-decorated electrode surface, with a current intensity of 13.9 μA and an anodic and cathodic peak separation ($\Delta E_p$) of 103.7 mV, at scan rate of 50 mV·s$^{-1}$ (Table 1). When the SPCE was decorated with Fe-MWCNT-e, the current intensity ($I_{p,a}$) increased up to 17.2 μA and the $\Delta E_p$ decreased down to 89.7 mV (Table 1). This change indicates that modification of the electrode surface favours the charge-transfer between the electrochemical probe and the electrode surface. The improved electrochemical response is related to the enhanced catalytic properties of the Fe-containing hybrid material. However, when the SPCE were modified with Fe@G-MWCNT, the current value resulted to be slightly worst ($I_{p,a}$=16.7 μA) respect to the Fe-MWCNT-modified electrode, even though both of them were much better than that from the MWCNT-modified SPCE. The apparent deterioration of the electrochemical properties is explained by the fact that graphene is coating the catalytic Fe nanoparticles, which slightly hinder the electron-transfer process. When the Fe-MWCNT and Fe@G-MWCNT-decorated SPCE were electrochemically reduced in sulphuric acid, following the protocol detailed in the experimental section, the electrochemical response was enhanced. The better electrochemical response of the Fe-MWCNT-modified SPCE is coming from the electrochemical reduction process that is removing the thin oxide layer from the natural oxidation process of Fe catalytic nanoparticles in air. The inset of Figure 3a shows an increase in the current intensity for Fe-MWCNT-e-modified SPCE with respect to the Fe-MWCNT-modified one, because of the mentioned electrochemical "activation process". Such an activation also occurs to the electrochemically reduced Fe@G-MWCNT respect to the same non reduced material, with the concomitant improvement on the electrochemical properties (results are not shown, but data are in Table 1). The formation of a 3D electrochemically induced graphene oxide network may account for such improvement [39].

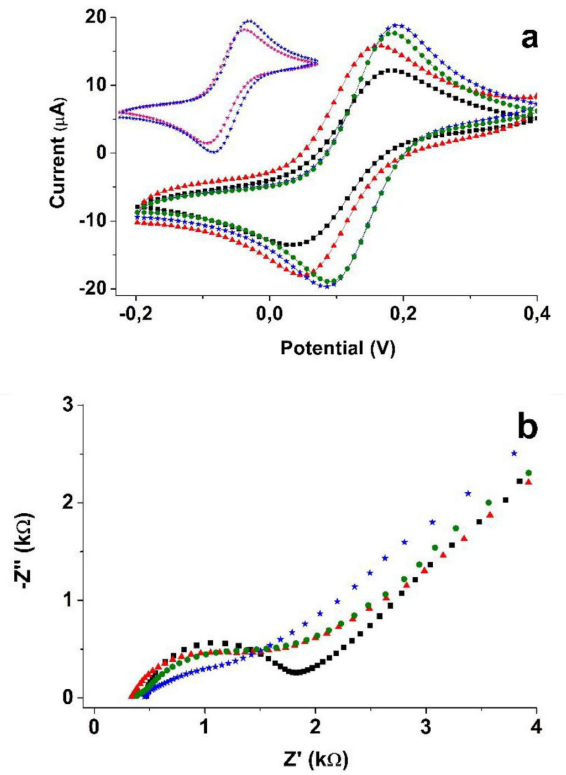


Fig. 3. **(a)** Cyclic voltammograms of MWCNT-modified SPCE in 1 mM $[Fe(CN)_6]^{3-}$/0.1 M $KNO_3$ solution and **(b)** Nyquist plot of a pH 7.4, 5.0 mM $[Fe(CN)_6]^{4-/3-}$/PBS 1X solution, in the frequency range from 50 kHz to 0.01 Hz, at an amplitude of 0.005 V for: SPCE (■), MWCNT (▲), Fe-MWCNT-e (★), Fe-MWCNT (★) and Fe@G-MWCNT-e (●). Inset are the CVs of Fe-MWCNT and Fe-MWCNT-e-modified SPCE.

The electroactive area ($A$) of the electrodes were calculated from the above mentioned CV experiments by using the Randles-Sevick equation [40,41] (Equation 1):

$$I_{p,a} = 0.4463nFAC\left(\frac{nFvD}{RT}\right)^{1/2} \quad (1)$$

Where, $I_{p,a}$ is the anodic peak current intensity, $n$ is the number of electrons involved in the electrochemical reaction, $A$ is surface area of the electrode (cm$^2$), $D$ is diffusion coefficient, $C$ is concentration of $K_3[Fe(CN)_6]$, $v$ is the scan rate, $R$ is the molar gas constant (8.314 J·K$^{-1}$·mol$^{-1}$) and $F$ is Faraday's constant (96480 C·mol$^{-1}$). For 1 mM $K_3[Fe(CN)_6]$/0.1 M $KNO_3$ at temperature, $T$=298.15 K, $n$=1 and $D$=7.26×10$^{-6}$ cm$^2$·s$^{-1}$, respectively.

In the present study, the electroactive area of the bare SPCE, MWCNT, Fe-MWCNT-e and Fe@G-MWCNT-e were calculated to be 7.1 mm$^2$, 8.6 mm$^2$, 10.6 mm$^2$ and 10.3 mm$^2$, respectively (Table 1). These results indicate the proper deposition of hybrid materials on the SPCE and the rougher surface of the hybrid decorated electrode surfaces respect to the MWCNT-decorated and bare SPCE counterparts. Higher the roughness, higher the ability to further host bioreceptors when developing biosensors.

To gain a better insight into the electrochemical performance of the modified electrodes, CV data were contrasted with EIS data. EIS of the bare SPCE,

MWCNT, Fe-MWCNT-e and Fe@G-MWCNT-e were studied in a pH 7.4, 5 mM $Fe(CN)_6^{3-/4-}$/PBS 1X solution. These data are represented as a Nyquist plot of Figure 3b.

This figure shows a decrease in the semicircle from the Nyquist plot when compared Fe-MWCNT-e with MWCNT, with $R_{ct}$ values of 1041 Ω and 1205 Ω, respectively. This decrease indicates that a higher electron-transfer occurs at Fe-MWCNT-e-modified SPCE caused by the catalytic properties of the Fe nanoparticles. When the SPCE is decorated with Fe@G-MWCNT-e, the $R_{ct}$ values slightly increase (1181 Ω) indicating that the graphene coating generates an added opposition to the current pass. Those results agree with the data from the CV, as discussed above.

Unlike the double layer capacitance, typically used in equivalent circuits, here we used instead the *CPE* element. *CPE* depends on a pre-exponential factor ($P$) and an exponent ($n$). $P$ values indicated an increase in the capacitive behavior of the system; and $n$ values for modified electrodes were less that one, consistent with a pseudo interfacial double layer capacitance at the electrode/electrolyte interface. *CPE* is used when protective coating systems are studied and takes into account factors that affect the capacitance of a system such as surface inhomogeneity [23,35,42]. Then, we used herein *CPE* in the model, as most of the protective coating materials that do not form a perfect barrier to water and ions [34], thereby allowing for some sort of diffusion through the coating. Finally, an increase in charge-transfer resistance and a decrease of the *CPE* values between the electrode and the solution ions indicate that graphene in Fe@G-MWCNT-e acts as a protective layer, thus limiting the electron-transfer process, while maintaining the conductivity of the Fe-MWCNT hybrid material (Table 1).

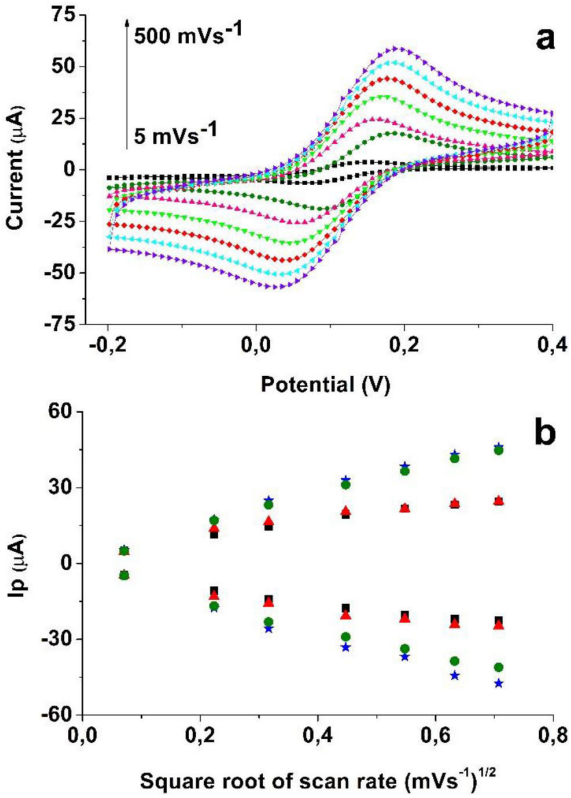


Fig. 4. **(a)** Cyclic voltammograms recorded at Fe@G-MWCNT-e in a 1 mM $[Fe(CN)_6]^{3-}$/0.1 M $KNO_3$ solution, at different scan rates. From inner to outer: 5, 50, 100, 200, 300, 400 mV·s$^{-1}$ and 500 mV·s$^{-1}$. CVs for the other materials are in the supporting information Figure S1. **(b)** Plot of cathodic ($I_{p,c}$) and anodic ($I_{p,a}$) peak current *vs* the square root of scan rates for SPCE (■), MWCNTs (▲), Fe-MWCNT-e (★) and Fe@G-MWCNT-e (●), respectively.

### 3.4 Heterogeneous Electron-Transfer Kinetics

CVs of the material-modified SPCEs in a 1 mM $[Fe(CN)_6]^{3-}$/0.1 M $KNO_3$ solution, at different scan rates were used to establish whether the electrochemical reaction is controlled by diffusion or adsorption and estimate their heterogeneous electron-transfer kinetics. Fe@G-MWCNT-e was studied in the electrochemical probe by varying the scan rate from 5 mV·s$^{-1}$ to 500 mV·s$^{-1}$ (Figure 4a). Studies of the scan rate variation for the SPCE, MWCNT, Fe-MWCNT-e are plotted in the Supporting Information (Figure S1), Figures a, b and c, respectively. In all cases, the $I_{p,c}$ increases as the scan rates does. The results showed a linear dependence of peak current with the square root of scan rate (Figure 4b), consistent with a diffusion-controlled redox process.

Because of the quasi-reversible behaviour of the $Fe^{3+/2+}$ at the material-modified electrode, the empirical method proposed by Nicholson [43] was used to calculate the heterogeneous rate constant, $k_s$. In order to use the Nicholson method, we need to know $\Psi$, which is a dimensionless charge-transfer parameter that is associated to the $\Delta E_p$, and proportional to $k_s$. The $\Psi$ values for each $\Delta E_p$ of the hybrid material-modified electrodes were obtained using the values reported by Nicholson [43], which correspond to that from the equation below (Figure S2 and Equation 2):

$$\Delta E_p = 96.032\Psi^{-0.234} \quad (2)$$

Thus, $k_s$ was calculated from Equation 3 [44]:

$$\Psi = \frac{k_s\left(\frac{D_0}{D_R}\right)^{\alpha/2}}{\sqrt{D_0\pi\upsilon F/RT}} \quad (3)$$

Where $D_0$ and $D_R$ are the diffusion coefficients of $[Fe(CN)_6]^{3-}$ and $[Fe(CN)_6]^{4-}$ assuming $(D_0/D_r=1)$ and $D_0 = 7.2\times10^{-6}$ cm$^2$·s$^{-1}$, α is the transfer coefficient, assuming $\alpha = 0.5$, because $I_{p,c}/I_{p,a} \approx 1$ [45].

Finally, the heterogeneous electron-transfer rate constants for each oxidation and reduction pairs were

calculated using Equation 3. The values of $k_s$ of $5.29\times10^{-2}$ cm·s$^{-1}$ and $3.21\times10^{-2}$ cm·s$^{-1}$ from Fe-MWCNT-e and Fe@G-MWCNT-e, respectively are higher than that from the MWCNT-decorated SPCE ($1.27\times10^{-2}$ cm·s$^{-1}$), (Table 1). These results are explained by the enhanced electron-transfer, promoted by the Fe-containing hybrid material. The heterogeneous electron-transfer rate constants from the Fe-MWCNT-e is therefore approximately 1.6, 4.1 and 4.4 fold higher than that from the Fe@G-MWCNT-e, MWCNT and the bare SPE, respectively. These results indicate the much faster electron-transfer kinetics at the Fe-MWCNT-e-modified electrode, and agree with the slightly higher charge-transfer resistance generated when coating the Fe nanoparticles with graphene flakes (Fe@G-MWCNT-e), which may limit the electron-transfer process.

### 3.5 Response of the Hybrid Material to $H_2O_2$

To reinforce the aforementioned results and demonstrate the potential that the hybrid-modified SPCE has for sensing purposes, we investigated the electrocatalytic activity of the hybrid materials toward $H_2O_2$ by both CV and amperometry. Figure 5a shows the CV of the bare SPCE, MWCNT, Fe-MWCNT-e and Fe@G-MWCNT-e in a 5.0 mM $H_2O_2$/0.1 M $KNO_3$ solution, at a scan rate of 50 mV s$^{-1}$. Voltammograms show a significant increase of anodic and cathodic peaks at the Fe-MWCNT-e and Fe@G-MWCNT-e-modified electrodes compared to the MWCNT alone and the bare SPCE, at the same $H_2O_2$ concentration. These results point out the high electrocatalytic activity of the hybrid material for oxidation/reduction of $H_2O_2$, which offers a way to detect $H_2O_2$ with high sensitivity.

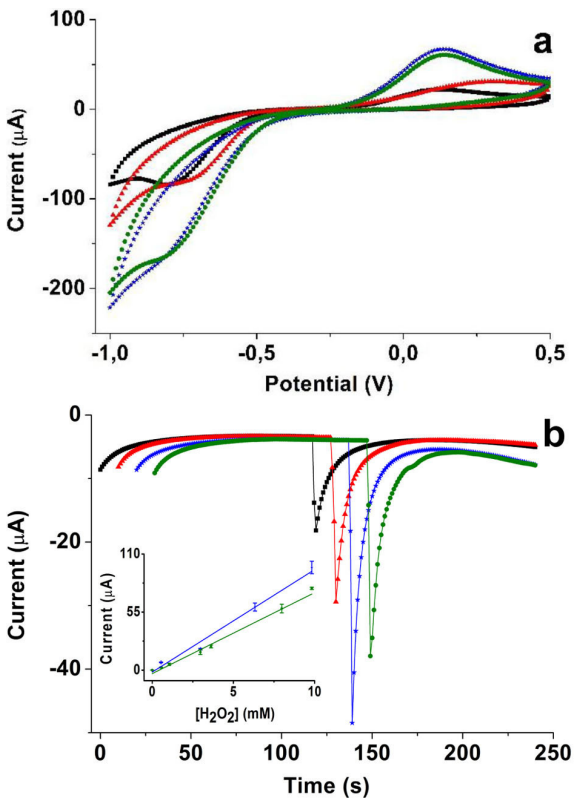


Fig. 5. **(a)** Cyclic voltammograms and **(b)** chronoamperograms for SPCE (■), MWCNT (▲), Fe-MWCNT-e (★) and Fe@G-MWCNT-e (●), respectively, in a 5 mM $H_2O_2$/0.1 M $KNO_3$ solution. Inset is the calibration curve for Fe-MWCNT-e and Fe@G-MWCNT-e in 0.5 mM to 10 mM $H_2O_2$/0.1 M $KNO_3$ solutions.

Figure 5b shows the amperometric response of the bare SPCE, MWCNT, Fe-MWCNT-e and Fe@G-MWCNT-e at a fixed potential of −0.68 V with addition of $H_2O_2$/0.1 M $KNO_3$ once the base line was established after 120 s. The chronoamperograms demonstrated that Fe-MWCNT-e produced a higher response with respect to the Fe@G-MWCNT-modified electrode. However, both of them were much better than those from the MWCNT-modified and the bare SPCE, respectively. The improved performance of the Fe-MWCNT-e observed from CV and amperometry is coming from its high catalytic activity of the reduced, free-exposed Fe nanoparticles. Fe@G-MWCNT-e showed an enhanced response with respect to the MWCNT alone, although slightly lower than that from the Fe-MWCNT-e hybrid material. Again, the graphene coating is accounting for such a slight decrease in the capability of the material for $H_2O_2$ reduction. A decrease of only 24.3 ± 7.1 % of the response was observed for Fe@G-MWCNT-e in one week, which was considerably lower than that from the Fe-MWCNT-e (51.9 ± 7.0 %) (Figure S3). These results demonstrate the protective effect of the graphene layer on the catalytic activity of iron nanoparticles. It is then expected that the protective layer of graphene to safeguard the Fe nanoparticles from oxidation, thus increasing the long-term stability of this hybrid architecture. The calibration curves for the Fe-MWCNT-e and Fe@G-MWCNT-e exhibited a linear range $H_2O_2$ concentration from 0.5 mM to 9.8 mM, with sensibility of 9.83 μA·mM$^{-1}$ and 7.97 μA·mM$^{-1}$; and LOD of 0.66 mM and 0.65 mM, respectively. Electrocatalytic oxidation of $H_2O_2$ at the Fe@G-MWCNT-e-modified electrode has been improved in terms of both long-stability and sensibility. Overall, Fe@G-MWCNT-modified electrode holds great potential for development of new (bio) sensors [46].

## 4 Conclusions

Electroanalysis of SPCEs modified with a Fe@G-MWCNT hybrid material was performed. Attachment of iron metallic nanoparticles on a MWCNT surface enhanced the electroactivity and promoted a faster electron-transfer process of the as-prepared hybrid material. Coating the iron nanoparticles with graphene layers demonstrated a slight increase in the electron-transfer resistance of the resultant hybrid material with respect to an uncoated one. However, the coating generated a protective layer that may prevent changes in the Fe oxidation

state, thus keeping the catalytic activity of the hybrid material, and increasing its long-term stability. Considering the enhanced electrocatalytic properties of the hybrid material with respect to the concomitant counterparts alone, faster electron-transfer rates and higher reactivity towards $H_2O_2$ were shown. Overall, the work opens an avenue for the development of more specific and highly sensitive (bio) sensors.

## Acknowledgements

J.O and D.S thank the financial support provided by COLCIENCIAS, Universidad de Antioquia and the Max Planck Society through the Cooperation agreement 566-1, 2014. J. G. acknowledges COLCIENCIAS and University of Antioquia for the support to the project 1115–715-51427.

## References

[1] V. Mani, S.-M. Chen, B.-S. Lou, *Int. J. Electrochem. Sci.* **2013**, *8*, 11641–11660.
[2] N. Yang, X. Chen, T. Ren, P. Zhang, D. Yang, *Sensors Actuators, B Chem.* **2015**, *207*, 690–715.
[3] H. Liu, Z. Fu, F. Song, Q. Liu, L. Chen, *RSC Adv.* **2017**, *7*, 3136–3144.
[4] X. Zhao, P. Zhang, Y. Chen, Z. Su, G. Wei, *Nanoscale* **2015**, *7*, 5080–5093.
[5] Y. Gong, X. Chen, Y. Lu, W. Yang, *Biosens. Bioelectron.* **2015**, *66*, 392–398.
[6] P. T. Yin, S. Shah, M. Chhowalla, K.-B. Lee, *Chem. Rev.* **2015**, *115*, 2483–2531.
[7] Z. Wang, Z. Dai, *Nanoscale* **2015**, *7*, 6420–6431.
[8] M. Carraro, S. Gross, *Materials (Basel)* **2014**, *7*, 3956–3989.
[9] N. Yang, X. Chen, T. Ren, P. Zhang, D. Yang, *Sensors Actuators B Chem.* **2015**, *207*, 690–715.
[10] E. M. Khalaf, S. A. Awad, *Int. J. Mater. Sci. Appl.* **2016**, *5*, 291–301.
[11] X. Yue, S. Pang, P. Han, C. Zhang, J. Wang, L. Zhang, *Electrochem. Commun.* **2013**, *34*, 356–359.
[12] J. Wen, Y. Xu, H. Li, A. Lu, S. Sun, *Chem. Commun.* **2015**, *51*, 11346–11358.
[13] T.-T. Tran, A. Mulchandani, *TrAC Trends Anal. Chem.* **2016**, *79*, 222–232.
[14] E. Mendoza, J. Orozco, C. Jiménez-Jorquera, A. B. González-Guerrero, A. Calle, L. M. Lechuga, C. Fernández-Sánchez, *Nanotechnology* **2008**, *19*, 75102.
[15] A. T. Lawal, *Mater. Res. Bull.* **2016**, *73*, 308–350.
[16] N. Akhtar, M. Y. Emran, M. A. Shenashen, H. Khalifa, T. Osaka, A. Faheem, T. Homma, H. Kawarada, S. A. El-Safty, *J. Mater. Chem. B* **2017**, *5*, 7985–7996.
[17] Y. Li, L. Zhang, M. Li, Z. Pan, D. Li, *Chem. Cent. J.* **2012**, *6*, 103.
[18] H. Khani, M. Kazem Rofouei, P. Arab, V. K. Gupta, Z. Vafaei, *J. Hazard. Mater.* **2010**, *183*, 402–409.
[19] M. Holzinger, A. Le Goff, S. Cosnier, *Front. Chem.* **2014**, *2*, 1–10.
[20] Y. Song, Y. Luo, C. Zhu, H. Li, D. Du, Y. Lin, *Biosens. Bioelectron.* **2016**, *76*, 195–212.
[21] J. Gallego, J. Tapia, M. Vargas, A. Santamaria, J. Orozco, D. Lopez, *Carbon N.Y.* **2017**, *111*, 393–401.
[22] W. Yang, K. R. Ratinac, S. P. Ringer, P. Thordarson, J. J. Gooding, F. Braet, *Angew. Chem. Int. Ed.* **2010**, *49*, 2114–2138.
[23] S. Singal, A. K. Srivastava, S. Dhakate, A. M. Biradar, R. Rajesh, *RSC Adv.* **2015**, *5*, 74994–75003.
[24] B. Unnikrishnan, Y.-L. Yang, S.-M. Chen, *Int. J. Electrochem. Sci.* **2011**, *6*, 3224–3237.
[25] C. Fernández-Sánchez, E. Pellicer, J. Orozco, C. Jiménez-Jorquera, L. M. Lechuga, E. Mendoza, *Nanotechnology* **2009**, *20*, 335501.
[26] A. Cavallini, G. De Micheli, S. Carrara, *Sens. Lett.* **2011**, *9*, 1838–1844.
[27] S. Mondal, D. Khastgir, *Composites Part A* **2017**, *102*, 154–165.
[28] N. Chauhan, C. S. Pundir, *Anal. Chim. Acta* **2011**, *701*, 66–74.
[29] J. Orozco, C. Jiménez-Jorquera, C. Fernández-Sánchez, *Bioelectrochemistry* **2009**, *75*, 176–181.
[30] V. V Mody, R. Siwale, A. Singh, H. R. Mody, *J. Pharm. Bioallied Sci.* **2010**, *2*, 282–9.
[31] J. Orozco, C. Jiménez-Jorquera, C. Fernández-Sánchez, *Electroanalysis* **2012**, *24*, 635–642.
[32] J. Gallego, G. Sierra, F. Mondragon, J. Barrault, C. Batiot-Dupeyrat, *Appl. Catal. A* **2011**, *397*, 73–81.
[33] J. Wanga, M. Pedreroa, H. Sakslund, O. Hammerichb, *Analyst* **1996**, *121*, 345–350.
[34] D. Du, X. Ye, J. Cai, J. Liu, A. Zhang, *Biosens. Bioelectron.* **2010**, *25*, 2503–2508.
[35] X. Dominguez-Benetton, S. Sevda, K. Vanbroekhoven, D. Pant, *Chem. Soc. Rev.* **2012**, *41*, 7228.
[36] B. Kumar, V. Bhalla, R. P. Singh Bhadoriya, C. R. Suri, G. C. Varshney, *RSC Adv.* **2016**, *6*, 75862–75869.
[37] I. Khan, U. J. Pandit, S. N. Limaye, *Electroanalysis* **2017**, *29*, 2423–2436.
[38] S. Mani, S. Cheemalapati, S. Chen, B. Devadas, *Int. J. Electrochem. Sci.* **2015**, *10*, 7049–7062.
[39] Y. Li, R. Zhao, L. Shi, G. Han, Y. Xiao, *RSC Adv.* **2017**, *7*, 53570–53577.
[40] J. Chen, R. Zhu, J. Huang, M. Zhang, H. Liu, M. Sun, L. Wang, Y. Song, *Analyst* **2015**, *140*, 5578–5584.
[41] B. Li, G. Pan, N. D. Avent, R. B. Lowry, T. E. Madgett, P. L. Waines, *Biosens. Bioelectron.* **2015**, *72*, 313–319.
[42] S. Skale, V. Doleček, M. Slemnik, *Corros. Sci.* **2007**, *49*, 1045–1055.
[43] R. S. Nicholson, *Anal. Chem.* **1965**, *37*, 1351–1355.
[44] P. A. Henry, A. S. Raut, S. M. Ubnoske, C. B. Parker, J. T. Glass, *Electrochem. Commun.* **2014**, *48*, 103–106.
[45] H. Alawdi, Thesis, College of Science and Mathematics, **2015**.
[46] V. Mani, T.-Y. Wu, S.-M. Chen, *J. Solid State Electrochem.* **2014**, *18*, 1015–1023.

Received: February 9, 2018
Accepted: April 23, 2018
Published online on ■■, ■■■

  

# FULL PAPER

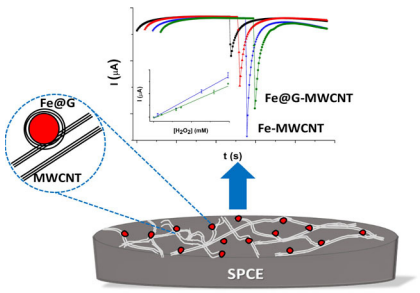


*D. Soto, M. Alzate, J. Gallego, J. Orozco**